Chemical Physics 502 (2018) 33–38

Contents lists available at ScienceDirect

Chemical Physics

journal homepage: www.elsevier.com/locate/chemphys

Angle dependence in slow photon photocatalysis using TiO_2 inverse opals

Mariano Curti [a,b], Gonzalo Zvitco [a], María Alejandra Grela [a,b], Cecilia B. Mendive [a,b,*]

[a] Departamento de Química, Facultad de Ciencias Exactas y Naturales, Universidad Nacional de Mar del Plata, Dean Funes 3350, 7600 Mar del Plata, Argentina
[b] Instituto de Investigaciones Físicas de Mar del Plata, CONICET/Facultad de Ciencias Exactas y Naturales, Universidad Nacional de Mar del Plata, Dean Funes 3350, 7600 Mar del Plata, Argentina

ARTICLE INFO

Article history:
Received 10 October 2017
In final form 9 January 2018
Available online 10 January 2018

Keywords:
Photonic photocatalysis
Slow photons
Inverse opals
TiO_2
Advanced oxidation processes
RCWA method

ABSTRACT

The slow photon effect was studied by means of the photocatalytic degradation of stearic acid over TiO_2 inverse opals. The comparison of the degradation rates over inverse opals with those obtained over disordered structures at different irradiation angles showed that the irradiation at the blue edge of the stopband leads to the activation of the effect, evidenced by an improvement factor of 1.8 ± 0.6 in the reaction rate for irradiation at 40°. The rigorous coupled-wave analysis (RCWA) method was employed to confirm the source of the enhancement; simulated spectra showed an enhancement in the absorption of the TiO_2 matrix that composes the inverse opal at a 40° irradiation angle, owing to an appropriate position of the stopband in relation to the absorption onset of TiO_2.

1. Introduction

Titanium dioxide, TiO_2, meets many of the requirements for its application as a photocatalytic material: it is inexpensive, it has low toxicity, and shows a relatively high activity when irradiated in the UV range [1]. Nonetheless, its lack of absorption in the visible region hinders the use of sunlight as the energy source for the desired photocatalytic processes [2]. Amongst the diverse strategies currently explored to improve the absorption of a material, its structuration as a photonic crystal [3] has emerged as a very interesting alternative, since it does not require to modify its chemical composition; therefore, the positive intrinsic properties of TiO_2 named above would not be affected. The strategy is based on the *slow photon* effect that arises from the spatial periodicity in the refractive index shown by photonic crystals [4]. This periodicity affects the propagation of photons, most notably, by reducing their group velocity at the edges of the photonic stopband. The resulting slow photons have been shown to be able to amplify the absorption capabilities of TiO_2 given an adequate overlap between the slow photon wavelength region, the emission spectrum of the irradiation source, and a region of low absorption of the material composing the photonic crystal [5]. Therefore, a careful tuning is needed for this condition to be met, since the slow photon regions are narrow and their precise location are difficult to predict from experimental transmission or reflectance spectra.

Previous works have shown that the slow photon effect can be operative both at the red [5,6] and at the blue edge [7–10] of the stopband. Although the red-edge slow photons can lead to a stronger amplification, the use of the blue-edge allows the photonic stopband to be located at longer wavelengths than the absorption onset of the material, thus minimizing reflection losses when using polychromatic light sources [11].

In this work we explore the use of the irradiation angle as the key variable to accurately control the activation of the slow photon effect in inverse opal photonic crystals. The comparison of photocatalytic degradation rates over TiO_2 inverse opals with respect to the rates shown by disordered but similarly porous TiO_2 structures allowed us to unambiguously identify the influence of the slow photons at the blue edge of the stopband. Since one of the most extended technological applications of photocatalysis are self-cleaning materials [12], we chose stearic acid as the model compound for the degradation reactions; specific aspects of its photo-oxidation have been studied by several research groups [12–16]. This degradation reaction presents the advantage of being a solid-state reaction, and thus we can rule out the influence of diffusional or surface area effects [17]. Moreover, the refractive index contrast within the inverse opal structure is improved with respect

* Corresponding author at: Departamento de Química, Facultad de Ciencias Exactas y Naturales, Universidad Nacional de Mar del Plata, Dean Funes 3350, 7600 Mar del Plata, Argentina.
E-mail address: cbmendive@mdp.edu.ar (C.B. Mendive).

https://doi.org/10.1016/j.chemphys.2018.01.007
0301-0104/

to aqueous phase reactions, where the cavities within the inverse opal are infilled with water, and thus a stronger slow photon effect can be expected in the solid-state reaction.

2. Materials and methods

The inverse opals (IO) preparation method is based on the Capillary Deposition Method [18,19]. Briefly, an aqueous suspension of monodisperse poly(methyl methacrylate) spheres was prepared by a surfactant-free emulsion polymerization reaction [20]; opal templates were then prepared by evaporation and self-assembly of the spheres within glass cells. Inverse opals were produced by infiltration of the templates with a suspension of TiO_2 nanoparticles, synthesized by a sol-gel reaction followed by peptization [21]. Finally, samples were calcined at 723 K (heating ramp: 1 K min^{-1}) for 180 min to remove the polymeric template. Disordered samples without photonic properties (labelled as "Mix") were prepared by a similar procedure, using a mixture of differently sized spheres for the templates synthesis instead of monodisperse spheres. The use of this mixture leads to a disordered structure in which the refractive index has no spatial periodicity.

UV–Visible spectra of the inverse opals were taken with an Agilent 8453 spectrophotometer in transmission mode. Scanning electron micrographs were taken with a Jeol JSM-6460LV microscope using an acceleration potential of 15 kV.

For the photocatalytic experiments stearic acid (Merck, 98%) was deposited over the inverse opals by spin-coating 200 μL of a 2.5 mmol L^{-1} solution in ethanol. The degradation reaction was followed via FT-IR spectroscopy using a PerkinElmer Spectrum BX II spectrophotometer in transmission mode, by monitoring the stearic acid absorption band at 2914 cm^{-1} (corresponding to the CH_2 asymmetric stretching [22]). A 3 W LED (λ_{max} = 400 nm; FWHM: 6 nm) was used as the excitation source. Its emitted photon flux for normal irradiation within the inverse opal area, as determined by chemical actinometry using phenylglyoxylic acid [23], was $I_0 = 2.35 \times 10^{16}$ s^{-1}. The irradiation angle was controlled with a homemade goniometer (Fig. 1) with a precision of ±1.5°. Three degradation experiments were performed with each sample type at each irradiation angle.

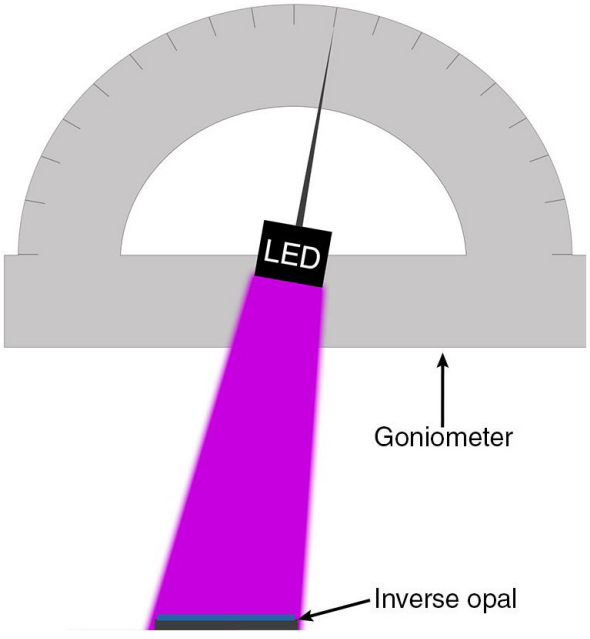

Fig. 1. Scheme of the experimental setup used for the photocatalytic degradations.

Between consecutive degradation cycles the samples were calcined for 60 min at 723 K in order to remove any unreacted stearic acid or intermediates that may have remained. This procedure did not modify the structural properties of the samples and allowed to obtain reproducible measurements. Furthermore, it removed the influence of inter-sample variability.

For the theoretical modelling of the inverse opals the freely available software package S^4 was used [24]. It allows to calculate reflectance, transmission and absorption spectra by implementing the rigorous coupled-wave analysis (RCWA) method, which has been shown to adequately describe the properties of inverse opals [11]. Although the method itself is exact, its implementation requires a finite number of Fourier coefficients to describe the structure, which, in turn, must be discretized in layers along the z-direction. The structural unit cell was discretized in 49 layers, while the Fourier series were truncated at 40 coefficients after checking the convergence of the calculated spectra. The simulated structure was composed of two materials: air, filling 74% of the volume with a refractive index of n_{air} = 1.00, and TiO_2, filling 26% of the volume and for which a refractive index of $n_{TiO_2} = 1.7$ was assumed. This number, lower than the generally accepted value for anatase TiO_2 ($n_{anatase}$ = 2.5), represents an incomplete filling of TiO_2 within the structure (as previously observed [25]), and was chosen by fitting the experimental stopband data to the modified Bragg equation (vide infra). The absorption of TiO_2 was taken into account by using a complex refractive index, i.e., $\bar{n} = n + i\kappa$, using the data given in Ref. [26] for values of κ. A cavity diameter of 250 nm was assumed in the inverse opals based on the fit to the Bragg equation, while six unit cells were used to model the inverse opal structure. Air was assumed as the surrounding medium above the structure, while a glass (n_{glass} = 1.5) substrate was modelled to be below the inverse opal. Unpolarized light was used throughout the simulations. As a reference material, a compact slab with the same absorption properties of TiO_2 and a thickness equal to 26% of that of the inverse opal (to take into account the TiO_2 filling fraction of the latter) was used. The real part of the refractive index was assumed to be n_{slab} = 1.38, in order to match the effective refractive index of the simulated inverse opals. Once having simulated the absorption spectra of inverse opals and of the reference slab, the absorption enhancement factor for inverse opals φ was calculated as:

$$\varphi = \int_0^\infty A_{IO}(\lambda)E_{LED}(\lambda)d\lambda \Big/ \int_0^\infty A_{Slab}(\lambda)E_{LED}(\lambda)d\lambda$$

where $A_{IO}(\lambda)$ represents the spectral absorptance (i.e., fraction of absorbed light; dimensionless) of the inverse opal at wavelength λ, $E_{LED}(\lambda)$ the spectral photon flux of the LED source (a.u. nm^{-1}), and $A_{Slab}(\lambda)$ the spectral absorptance of the reference slab (dimensionless).

3. Results and discussion

Two types of samples where used throughout this work: inverse opals prepared from monodisperse PMMA spheres (IO), and disordered films prepared from a mixture of spheres (Mix). The infiltration step was performed with a suspension of preformed nanoparticles, which greatly improves the optical, mechanical, and photonic properties of the inverse opals with respect to the commonly used liquid precursor infiltration [27].

The structure of the samples was assessed by scanning electron microscopy measurements. In the inverse opals (Fig. 2a) the cavities form regular arrangements, yielding a material with a spatial periodicity in its refractive index. Contrarily, the samples prepared from a mixture of differently sized spheres show a completely random structure (Fig. 2b).

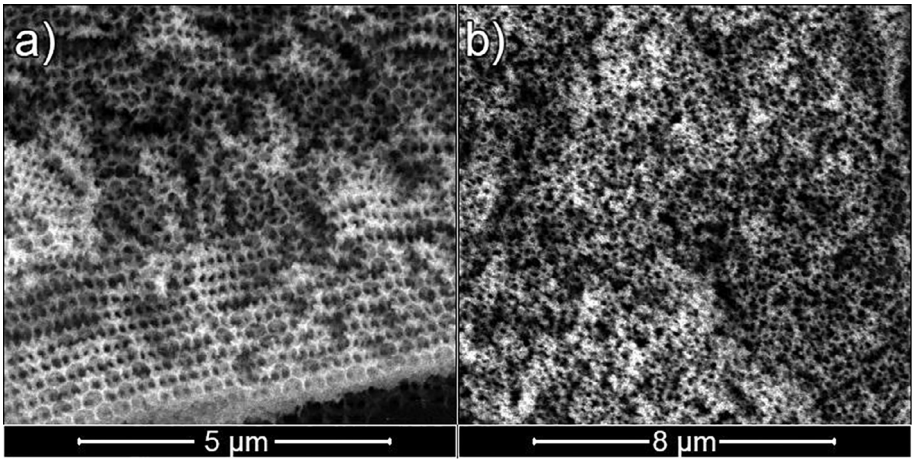

Fig. 2. Scanning Electron Microscopy images of (a) an inverse opal (lateral view) and (b) a disordered Mix sample.

In Fig. 3a the UV–visible transmission spectra of IO are shown at different irradiation angles. The stopband position shifts to shorter wavelengths when increasing the angle, in agreement with the photonic band structure of inverse opals [4].

Fig. 3b shows the position of the stopband maximum as a function of the incident light angle for IO samples. The measured range, 0–30°, can be extrapolated by fitting to the modified Bragg law for the first order diffraction:

$$\lambda = 2\sqrt{2/3}D\left[\left(\phi n_{TiO_2}^2 + (1-\phi)n_{medium}^2\right) - \sin^2\theta\right]^{1/2}$$

where D is the diameter of the cavities, ϕ the filling fraction of TiO_2 in the structure, n_{medium} the refractive index of air, and θ the incident angle of light with respect to the normal. A diameter of 247 nm was calculated for the cavities through the fitting to the equation, in broad agreement with the SEM measurements. The calculated TiO_2 filling fraction, of 13.9%, is considerably lower than the expected value of 26%. This discrepancy has been observed before [25] and can be explained on the basis of an incomplete filling of the opal template voids [17].

In order to avoid the interference of environmental factors such as temperature and humidity (which have shown to affect the stearic acid degradation rate [16,28]) or a possible interference by the variation in the effective thickness of the samples at different irradiation angles, two simultaneous reactions were performed for each angle: one over an IO sample, and the other over a Mix sample. Due to the experimental design, in the absence of any photonic effect the relation $\Delta_{IO}^{60\ min}/\Delta_{Mix}^{60\ min}$ (where $\Delta_{sample}^{60\ min}$ represents the amount of stearic acid degraded over 60 min over a given sample) should be independent of the irradiation angle; the activation of the slow photon effect would manifest as an anomaly in this ratio. The emission spectrum of the excitation source is shown in Fig. 3a, and is centered at 400 nm. Therefore TiO_2 is excited in the limit of its bandgap, where its absorption is rather low and thus can be strongly amplified by the slow photon effect.

Fig. 4 shows the kinetic profile of the stearic acid degradation reaction over inverse opals. The concentration decays in a monoexponential fashion; the reason of this fact will be discussed below.

Fig. 5 shows the $\Delta_{IO}^{60\ min}/\Delta_{Mix}^{60\ min}$ ratio measured as a function of the irradiation angle. At normal irradiation (0° angle) this ratio is 0.5 ± 0.1, which means that after 60 min Mix samples are able to degrade almost double the amount of stearic acid than IO samples. The random packing of differently sized spheres (as those used for the preparation of the Mix templates) usually leads to low packing fractions [29]. This results in an increased amount of TiO_2 in Mix samples after the infiltration procedure in comparison with IO samples, and may explain the larger efficiency of the former under normal irradiation.

Irradiation at 10°, 20°, 30° and 50° leads to a similar situation: the average ratio $\Delta_{IO}^{60\ min}/\Delta_{Mix}^{60\ min}$ for these angles is 0.6 ± 0.2. However, when the irradiation is performed at 40°, the photoactivity of the samples is reversed: for 40°, the ratio is 1.8 ± 0.6, a value that shows that for this angle IO samples are able to degrade an amount of almost double of stearic acid than Mix samples in 60 min. This

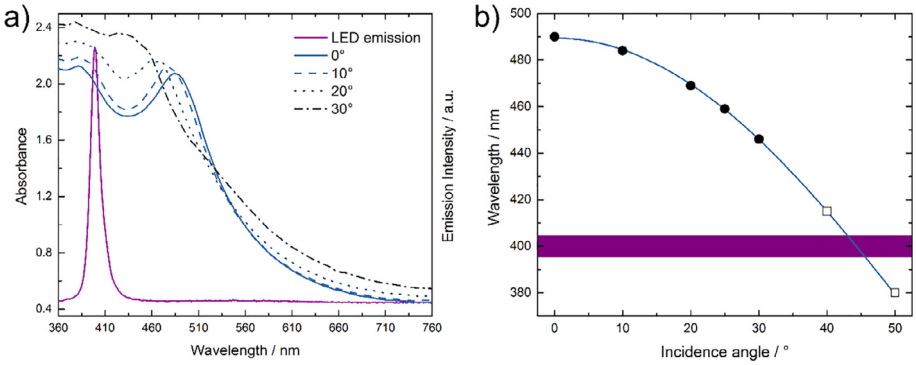

Fig. 3. (a) UV–visible absorption spectra, measured in transmission mode, of IO samples at different incidence angles. Also shown is the emission spectrum of the light source used in the photocatalytic experiments. (b) Position of the stopband center as a function of the irradiation angle. Solid circles show experimental data while empty boxes show the extrapolated values. The blue line shows the fitting to the modified Bragg equation while the violet region denotes the emission range of the light source. (For interpretation of the references to colour in this figure legend, the reader is referred to the web version of this article.)

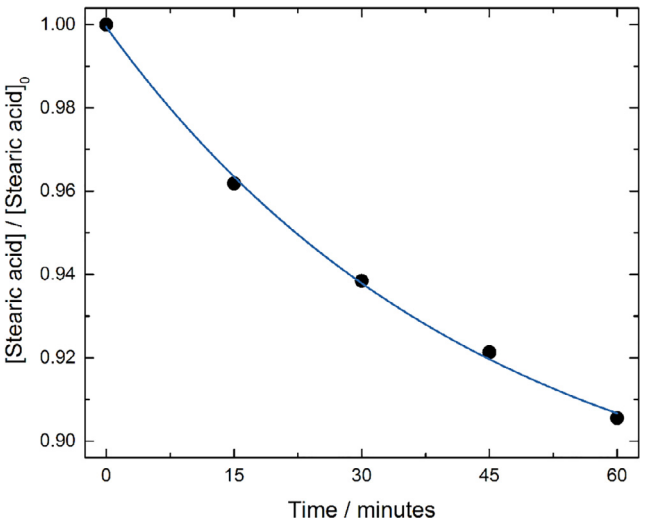

Fig. 4. Kinetic profile of the stearic acid photocatalytic degradation over IO samples under UV (λ_{max}=400 nm) irradiation. The blue line shows the monoexponential fit to the data. (For interpretation of the references to colour in this figure legend, the reader is referred to the web version of this article.)

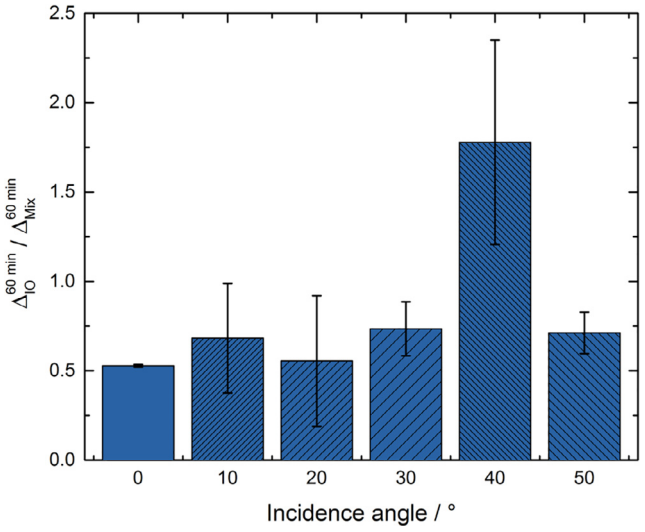

Fig. 5. Ratio of the amount of stearic acid degraded after 60 min over IO samples in relation to the amount degraded in 60 min over Mix samples, as a function of the irradiation angle.

variation shows the presence of the slow photon effect, since the angle-resolved comparison of the inverse opal with the disordered reference removes the influence of factors such as temperature, humidity, porosity, surface area, or emission intensity of the light source.

The emission spectrum of the irradiation source has its maximum *ca.* 15 nm towards shorter wavelengths with respect to the stopband of IO samples when they are irradiated at a 40° angle. Consequently, both the source emission and the material absorption overlap with the blue edge of the stopband, allowing the slow photons to amplify the small absorption shown by TiO_2 between 380 and 400 nm [30].

The light absorption amplification by the slow photons at the blue edge of the stopband has been studied by Deparis et al. by means of simulations based on the RCWA method [11], which has the valuable capability of taking into account the absorption of the materials [31]. We applied the same technique to gain

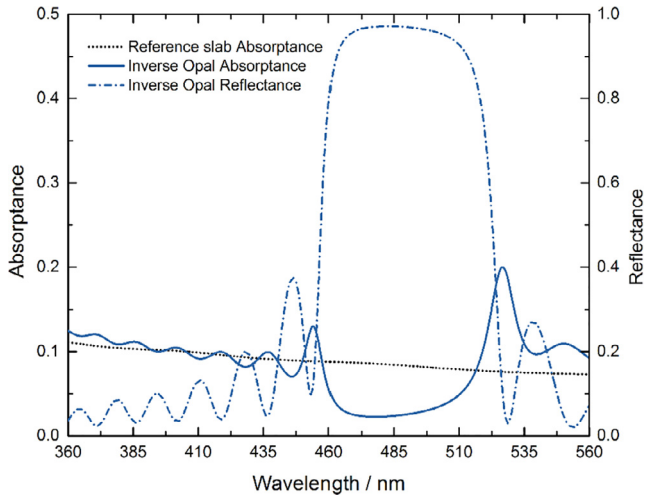

Fig. 6. Reflectance spectrum of an inverse opal as calculated by the RCWA method at 0° irradiation angle, and absorptance spectra of the inverse opal and the reference slab.

further insights on the slow photon effect in our particular case. The method was used to calculate reflectance and absorptance (i.e., fraction of absorbed light) spectra of inverse opals akin to those used in the experiments, and of reference slabs with the same amount of absorbing material but without any periodicity in its refractive index.

As a first step, in order to simplify the problem and have a clear picture of the slow photon effect, we set the complex part of the refractive index as a constant (κ = 0.1), independent of wavelength (i.e., a constant absorption spectrum). Fig. 6 shows the simulated reflectance spectrum for the inverse opal, which shows a stopband maximum at 490 nm, in agreement with the experimental transmission spectrum (Fig. 3). The figure also shows the absorptance spectra of both the inverse opal and the reference slab. These simulations clearly show that the slow photons are capable of enhancing the absorption of the material: at both edges of the stopband the absorptance of the inverse opal shows a sharp increase. At the red edge of the stopband the absorption of the inverse opal surpasses that of the reference slab by a factor of 2.7, while at the blue edge this value is 1.6. This is in agreement with previous experimental and theoretical results [7,11], which showed a stronger slow photon effect at the red edge of the stopband owing to a stronger localization of the electric field in the TiO_2 matrix. Our simulation is useful for determining the exact position of the effect in a perfect (i.e., without defects of any type) inverse opal; the calculated spectra show that the effect is active at the immediate edges of the stopband. Furthermore, it shows, as previously measured [32,33], that the absorption of photons within the stopband range is hindered due to the high reflectance of the inverse opal in this region.

In order to match the experimental conditions employed in this work, in a second step we used experimental values [26] for the complex part of the refractive index, to properly model the absorption of TiO_2.

Fig. 7a shows the reflectance and absorptance spectra of the simulated inverse opal, together with the absorptance of the reference slab, at an irradiation angle of 0°. The stopband is far away from the absorption onset, and thus the slow photons have no effect on the absorption of the inverse opal, yielding an absorptance spectrum practically identical to that of the reference slab. Fig. 7b depicts the same spectra, but now calculated at an irradiation angle of 40°, at which we observed the slow photon effect. The stopband now has shifted to 419 nm (in agreement with the

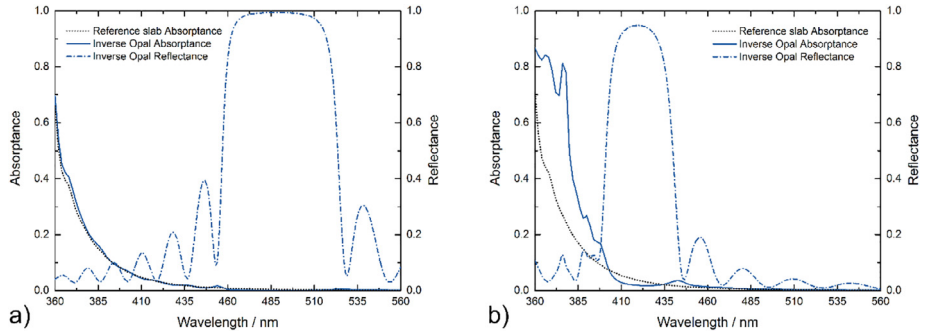

Fig. 7. Reflectance and absorptance spectra of an inverse opal as calculated by the RCWA method, together with the absorptance spectrum of a reference slab, (a) at a 0° irradiation angle, and (b) at a 40° irradiation angle.

experimental extrapolated value, Fig. 3b), and the slow photons at the blue edge are capable of improving the absorption: the absorptance in the irradiated region, 390–410 nm, is greatly enhanced with respect to the reference slab, explaining the observed enhancement in the stearic acid degradation rate when using a 40° irradiation angle. The absorption enhancement factor φ due to the slow photons, calculated from the overlap of the emission spectrum and the absorption spectra (see Section 2), is 1.48, in agreement with the experimental result of 1.8 ± 0.6 for the degradation of stearic acid. Therefore, the RCWA method explains the observed enhancement in the photocatalytic degradation rate of stearic acid.

4. Conclusions

The evaluation of the photocatalytic degradation rates of stearic acid over TiO_2 inverse opals in comparison to disordered structures as a function of the irradiation angle unequivocally showed the influence of the slow photon effect. For an irradiation angle of 40° an improvement by a factor of 1.8 ± 0.6 was observed with respect to the reference sample. The modelling of the system by means of the rigorous coupled-wave analysis method helped to understand the underlying mechanism of the slow photon effect.

Acknowledgements

The authors acknowledge MINCYT-FONCYT (Proj. Nr. PICT-2683 and PICT-1456) and UNMdP (Proj. Nr. EXA-701/14 and EXA-794/16) for the financial support. CBM and MAG are members of the research staff of Consejo Nacional de Investigaciones Científicas y Técnicas (CONICET). MC is grateful to CONICET for his doctoral and postdoctoral scholarships.

References

[1] J. Schneider, M. Matsuoka, M. Takeuchi, J. Zhang, Y. Horiuchi, M. Anpo, D.W. Bahnemann, Understanding TiO_2 photocatalysis: mechanisms and materials, Chem. Rev. 114 (2014) 9919–9986, https://doi.org/10.1021/cr5001892.
[2] S. Banerjee, S.C. Pillai, P. Falaras, K.E. O'Shea, J.A. Byrne, D.D. Dionysiou, New insights into the mechanism of visible light photocatalysis, J. Phys. Chem. Lett. 5 (2014) 2543–2554, https://doi.org/10.1021/jz501030x.
[3] J.I.L. Chen, G. von Freymann, S.Y. Choi, V. Kitaev, G.a. Ozin, Slow photons in the fast lane in chemistry, J. Mater. Chem. 18 (2008) 369–373, https://doi.org/10.1039/b708474a.
[4] J.D. Joannopoulos, S.G. Johnson, J.N. Winn, R.D. Meade, Photonic Crystals: Molding the Flow of Light, Princeton University Press, 2011.
[5] J.I.L. Chen, G. von Freymann, S.Y. Choi, V. Kitaev, G.a. Ozin, Amplified photochemistry with slow photons, Adv. Mater. 18 (2006) 1915–1919, https://doi.org/10.1002/adma.200600588.
[6] T.K. Rahul, N. Sandhyarani, Nitrogen-fluorine co-doped titania inverse opals for enhanced solar light driven photocatalysis, Nanoscale 7 (2015) 18259–18270, https://doi.org/10.1039/C5NR04663G.
[7] M. Wu, J. Liu, J. Jin, C. Wang, S. Huang, Z. Deng, Y. Li, B.-L. Su, Probing significant light absorption enhancement of titania inverse opal films for highly exalted photocatalytic degradation of dye pollutants, Appl. Catal. B: Environ. 150–151 (2014) 411–420, https://doi.org/10.1016/j.apcatb.2013.12.037.
[8] J.I.L. Chen, G.a. Ozin, Tracing the effect of slow photons in photoisomerization of azobenzene, Adv. Mater. 20 (2008) 4784–4788, https://doi.org/10.1002/adma.200801833.
[9] X. Li, X. Zhang, X. Zheng, Y. Shao, M. He, P. Wang, X. Fu, D. Li, A facile preparation of $ZnGa_2O_4$ photonic crystals with enhanced light absorption and photocatalytic activity, J. Mater. Chem. A 2 (2014) 15796–15802, https://doi.org/10.1039/C4TA03333G.
[10] R. Mitchell, R. Brydson, R.E. Douthwaite, Enhancement of hydrogen production using photoactive nanoparticles on a photochemically inert photonic macroporous support, Phys. Chem. Chem. Phys. 17 (2015) 493–499, https://doi.org/10.1039/C4CP04333B.
[11] O. Deparis, S.R. Mouchet, B.-L. Su, Light harvesting in photonic crystals revisited: why do slow photons at the blue edge enhance absorption?, Phys Chem. Chem. Phys. 17 (2015) 30525–30532, https://doi.org/10.1039/C5CP04983K.
[12] A. Mills, J. Wang, Simultaneous monitoring of the destruction of stearic acid and generation of carbon dioxide by self-cleaning semiconductor photocatalytic films, J. Photochem. Photobiol. A: Chem. 182 (2006) 181–186, https://doi.org/10.1016/j.jphotochem.2006.02.010.
[13] P. Sawunyama, L. Jiang, A. Fujishima, K. Hashimoto, Photodecomposition of a Langmuir-Blodgett film of stearic acid on TiO_2 film observed by in situ atomic force microscopy and FT-IR, J. Phys. Chem. B 101 (1997) 11000–11003, https://doi.org/10.1021/jp9730095.
[14] P. Sawunyama, A. Fujishima, K. Hashimoto, Photocatalysis on TiO_2 surfaces investigated by atomic force microscopy: photodegradation of partial and full monolayers of stearic acid on TiO_2(1 1 0), Langmuir 15 (1999) 3551–3556, https://doi.org/10.1021/la9814440.
[15] A. Mills, A. Lepre, N. Elliott, S. Bhopal, I.P. Parkin, S.A. O'Neill, Characterisation of the photocatalyst Pilkington Activ™: a reference film photocatalyst?, J Photochem. Photobiol. A: Chem. 160 (2003) 213–224, https://doi.org/10.1016/S1010-6030(03)00205-3.
[16] E.I. Cedillo-González, C. Mugoni, M. Montorsi, C. Siligardi, Evaluation of the correlations between temperature, humidity, incident UV light and the photocatalytic activity of TiO_2 films using a rationale approach, Appl. Surf. Sci. 378 (2016) 73–79, https://doi.org/10.1016/j.apsusc.2016.03.202.
[17] J.I.L. Chen, G.a. Ozin, Heterogeneous photocatalysis with inverse titania opals: probing structural and photonic effects, J. Mater. Chem. 19 (2009) 2675, https://doi.org/10.1039/b900965e.
[18] H.-L. Li, W. Dong, H.-J. Bongard, F. Marlow, Improved controllability of opal film growth using capillaries for the deposition process, J. Phys. Chem. B 109 (2005) 9939–9945, https://doi.org/10.1021/jp050385d.
[19] M. Curti, C.B. Mendive, M.A. Grela, D.W. Bahnemann, Stopband tuning of TiO_2 inverse opals for slow photon absorption, Mater. Res. Bull. 91 (2017) 155–165, https://doi.org/10.1016/j.materresbull.2017.03.061.
[20] D. Zou, S. Ma, R. Guan, M. Park, L. Sun, J.J. Aklonis, R. Salovey, Model filled polymers. V. Synthesis of crosslinked monodisperse polymethacrylate beads, J. Polym. Sci. Part A: Polym. Chem. 30 (1992) 137–144, https://doi.org/10.1002/pola.1992.080300118.
[21] Y.G. Seo, H. Lee, K. Kim, W. Lee, Transparent thin films of anatase titania nanoparticles with high refractive indices prepared by wet coating process, Mol. Cryst. Liq. Cryst. 520 (2010) 201–208, https://doi.org/10.1080/15421400903584424.
[22] T. Minabe, D.A. Tryk, P. Sawunyama, Y. Kikuchi, K. Hashimoto, A. Fujishima, TiO_2-mediated photodegradation of liquid and solid organic compounds, J. Photochem. Photobiol. A: Chem. 137 (2000) 53–62, https://doi.org/10.1016/S1010-6030(00)00350-6.
[23] A. Defoin, R. Defoin-Straatmann, K. Hildenbrand, E. Bittersmann, D. Kreft, H.J. Kuhn, A new liquid phase actinometer: quantum yield and photo-CIDNP study of phenylglyoxylic acid in aqueous solution, J. Photochem. 33 (1986) 237–255, https://doi.org/10.1016/0047-2670(86)87038-1.

[24] V. Liu, S. Fan, S^4: a free electromagnetic solver for layered periodic structures, Comput. Phys. Commun. 183 (2012) 2233–2244, https://doi.org/10.1016/j.cpc.2012.04.026.
[25] R.C. Schroden, M. Al-Daous, C.F. Blanford, A. Stein, Optical properties of inverse opal photonic crystals, Chem. Mater. 14 (2002) 3305–3315, https://doi.org/10.1021/cm020100z.
[26] B.S. Richards, Single-material TiO_2 double-layer antireflection coatings, Sol. Energy Mater. Sol. Cells 79 (2003) 369–390, https://doi.org/10.1016/S0927-0248(02)00473-7.
[27] M. Curti, G. López Robledo, C. dos Santos Claro, J. Ubogui, C.B. Mendive, Characterization of titania inverse opals prepared by two distinct infiltration approaches, Mater. Res. Bull. 101 (2018) 12–19, https://doi.org/10.1016/j.materresbull.2017.12.035.
[28] S. Costacurta, G.D. Maso, R. Gallo, M. Guglielmi, G. Brusatin, P. Falcaro, Influence of temperature on the photocatalytic activity of sol−gel TiO_2 films, ACS Appl. Mater. Interfaces 2 (2010) 1294–1298, https://doi.org/10.1021/am100149e.
[29] N.D. Aparicio, A.C.F. Cocks, On the representation of random packings of spheres for sintering simulations, Acta Metall. Mater. 43 (1995) 3873–3884, https://doi.org/10.1016/0956-7151(95)90170-1.
[30] J. Liu, H. Zhao, M. Wu, B. Van der Schueren, Y. Li, O. Deparis, J. Ye, G.A. Ozin, T. Hasan, B.-L. Su, Slow photons for photocatalysis and photovoltaics, Adv. Mater. (2017) 1605349, https://doi.org/10.1002/adma.201605349.
[31] M. Curti, J. Schneider, D.W.W. Bahnemann, C.B.B. Mendive, Inverse opal photonic crystals as a strategy to improve photocatalysis: underexplored questions, J. Phys. Chem. Lett. 6 (2015) 3903–3910, https://doi.org/10.1021/acs.jpclett.5b01353.
[32] J. Chen, G. von Freymann, S.Y. Choi, V. Kitaev, G.A. Ozin, Amplified photochemistry with slow photons, Adv. Mater. 18 (2006) 1915–1919, https://doi.org/10.1002/adma.200600588.
[33] J.I.L. Chen, G.A. Ozin, Tracing the effect of slow photons in photoisomerization of azobenzene, Adv. Mater. 20 (2008) 4784–4788, https://doi.org/10.1002/adma.200801833.